

An Itinerant Oscillator model with cage inertia for mesorheological granular experiments

Antonio Lasanta and Andrea Puglisi

CNR-ISC and Dipartimento di Fisica, Università La Sapienza, p.le A. Moro 2, 00185 Rome, Italy

Recent experiments with a rotating probe immersed in weakly fluidized granular materials show a complex behavior on a wide range of timescales. Viscous-like relaxation at high frequency is accompanied by an almost harmonic dynamical trapping at intermediate times, with possibly anomalous long time behavior in the form of super-diffusion. Inspired by the Itinerant Oscillator model for diffusion in molecular liquids, and other models with coupled thermostats acting at different timescales, here we discuss a new model able to account for fast viscous relaxation, dynamical trapping and super-diffusion at long times. The main difference with respect to liquids, is a non-negligible cage inertia for the surrounding (granular) fluid, which allows it to sustain a slow but persistent motion for long times. The computed velocity power density spectra and mean-squared displacement qualitatively reproduce the experimental findings. We also discuss the linear response to external perturbations and the tail of the distribution of persistency time, which is associated with superdiffusion, and whose cut-off time is determined by cage inertia.

PACS numbers: 45.70.-n,05.40.-a,47.57.Gc

I. INTRODUCTION.

Granular materials share analogies with condensed “molecular” matter, but often escape its well-established theoretical approaches [1, 2]. Equilibrium statistical physics may suggest only very approximate ideas about the qualitative behavior of granular media in strongly fluidized steady states and dramatically fails in the extreme case of static or quasi-static regimes. Continuum descriptions for dense flows lack first-principle constitutive relations [3, 4], while more refined kinetic theories (e.g. mode-coupling) must be carefully adapted to take into account some fundamental peculiarities, such as the breaking of time-reversal invariance and the relevance of the inertia of the medium [5]. The building up of granular hydrodynamics from “microscopic” models (ie. where all grains are described) is a promising program, but for the moment its success is limited to dilute regimes and rests upon the (uncertain) separation between fast and slow scales [6–8].

Our understanding of the liquid state of granular matter, being in the middle between two opposite worlds (the very fast “granular gases” and the very slow “granular glasses”), is even more incomplete and may benefit from simplified effective models. An important insight is provided by experiments, where the “liquid” state is realized through the application of some mild shaking leading to a slowly mixing flow with strong correlations and long but finite relaxation times [9–11]. When the longest relaxation time overcomes the experimental times, one may say to have reached a *transition point*, entering into a sort of - empirically defined - solid or glassy state [12–14]. We do not intend to directly address such a transition: however some of our results, in the following, concern also this delicate point.

The present paper aims at discussing a simplified *linear* model which is able to reproduce some noticeable

phenomena observed in a granular liquid state [11]. In particular our ambition is to propose a minimal model which exhibits a transient cage effect and super-diffusion at later times. Caging is a common hallmark of diffusion in dense liquids [15] and it is usually found in granular systems at large packing fractions [5, 16, 17]. Superdiffusion is much less common in liquids, it seems rather a peculiar effect of granular systems [13, 14], however it is rarely seen and hardly explained: below the jamming transition it has been observed in [14], above such a transition it was seen in [13] where it was imputed to “zero”-modes of the host fluid, or in [18] where the mechanism of Taylor dispersion was involved, or in [19] explained by a turbulence-like cascade effect. A universal scenario for anomalous diffusion is lacking [20], but certainly it is the signal of an enduring memory. A family of phenomenological models for anomalous diffusion includes fractional Fokker-Planck equations [21], where an immediate physical interpretation is not always at hand. The observations in [11] were better explained through a phenomenological continuous time random walk model for the *velocity* [22], with a power-law-decaying distribution of persistency times which was confirmed by experimental measurements. Such a model however could not explain the cage effect (which is a sub-diffusive behavior at earlier times) and was, therefore, adopted to match only partially the experimental results, in particular the slow time-scales. The model presented here, on the contrary, aims at offering a unifying picture for the two phenomena, and highlights the essential role of the “cage inertia”, which is the origin of long-time memory.

The organisation of the paper is as follows. In Section II we summarize the results of a recent experiment, carried on by one of the authors, where time correlations and mean squared displacement of a probe were measured, interpreted under the light of a first simplified model. In Section III we propose the new Itinerant Oscillator model with cage inertia, with a discussion of

its motivation. In Section IV we report the main formula for static quantities in the steady state. In Section V, we discuss two-time quantities in the steady (time-translation invariant) state, including the velocity spectrum, the mean squared displacement, linear response and, computed only numerically, the distribution of persistency times. Conclusions and perspectives are drawn in Section VI.

II. A RECENT EXPERIMENT ON GRANULAR MESORHEOLOGY

The granular liquid state is characterized by the emergence of many time-scales, associated with the complex and collective relaxation behavior of grains. A window into those time-scales may be open by studying the dynamics of a diffusing impurity, both in experiments and in simulations [11, 23]. A recent experimental study [11] has offered a new picture in a wide range of time-scales, from 10^{-3} s up to 10^3 s and more, revealing a non trivial scenario. In the experimental setup, sketched in Fig. 1A the “impurity” was constituted by an immersed blade (with momentum of inertia I) who could rotate around a fixed vertical axis under the kicks from the grain of a vibrofluidized granular medium. The dynamics of the angular velocity $\omega(t)$ of the blade and its absolute angular position $\theta(t) = \int_0^t ds \omega(s)$, was studied in different regimes of density and intensity of vibration. In Fig. 1B, the velocity power density spectrum (vpds) $S(f) = \frac{1}{2\pi t_{TOT}} |\int_0^{t_{TOT}} \omega(t) e^{i(2\pi f)t} dt|^2$ is presented and its salient features are highlighted in two opposite limits, which are the gas and the cold liquid. We remind that the vpds is the Fourier transform of the velocity autocorrelation function (vacf) and that its $f \rightarrow 0^+$ limit is the self-diffusion coefficient, i.e. $D_\infty = \pi \lim_{f \rightarrow 0^+} S(f)$. We also recall that relations exist, under certain approximations, between the vpds and the intermediate scattering function which - in liquids - is typically accessed through neutron scattering experiments [24].

In the gas limit, when the packing fraction is low and the average energy per grain is high, the probe velocity autocorrelation (vacf) is close to a simple exponential decay $\sim e^{-t/\tau_{gas}}$, ruled by a single relaxation time τ_{gas} : in this limit the vpds takes the form of a Lorentzian $S(f) \propto \frac{1}{\pi\gamma} [1 + (2\pi I f / \gamma)^2]$ with $\gamma = I / \tau_{gas}$.

In the cold liquid limit, when the packing fraction is high (larger than 30 – 35%) and the average energy per grain is small (but still in an “ergodic” phase), the observed vpds strongly deviates from the Lorentzian. Ignoring a mechanical resonance due to the mounting plate at $\sim 10^2 Hz$, it displays four different regions: at high frequency (region IV) it decays with a negative power law equal or smaller than 2; in region III it shows a smooth parabolic maximum (centered near $\sim 10 Hz$, reminiscent of a harmonic confinement (“cage”)); in region II it stabilizes on a short plateau, which suggests a loss of memory (as in the plateau of the Lorentzian which marks the on-

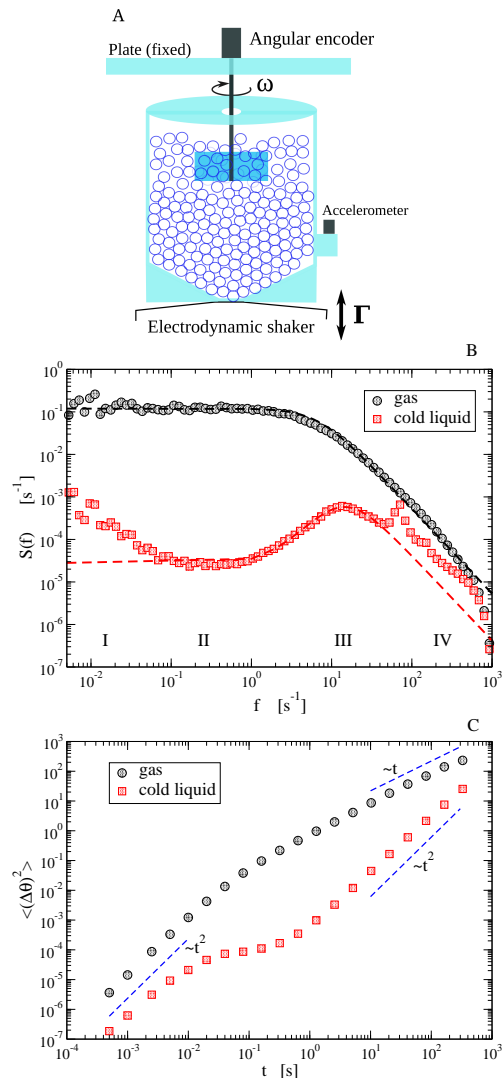


FIG. 1. A: sketch of the experiment reported in [11]. B: experimental data of the vpds for the gas case and the “cold liquid” case, together with predictions (dashed lines) from the incomplete model, Eq. (1). C: experimental data of the msd for both cases, together with dashed lines useful as guides for the eye.

set of normal diffusion); finally region I, perhaps the most surprising one, shows an increasing $S(f)$ for $f \rightarrow 0^+$, signaling a problem with the finiteness of the self-diffusion coefficient D_∞ . A few longer experiments (12 hours) were conducted, showing a slow crossover toward a new higher plateau at very low frequencies. The study of the mean squared displacement (msd), see Fig. 1C confirmed that the four regions of the cold liquid case correspond, respectively, to short-time ballistic (free) motion (IV), dynamical arrest due to caging (III), later relaxation of the cage (II) and “final” superdiffusive behavior (I).

In [11] a first model was proposed to account for regions II-III-IV of the vpds in the cold liquid limit. The model, which was inspired by a model for diffusion in cold liquids called Itinerant Oscillator model [25–27], also recently

used to describe microrheology in living matter [28], describes the evolution in time of the angular velocity of the probe $\omega(t)$ and its angular position $\theta(t) = \int_0^t ds\omega(s)$, according to the following stochastic equations of motion:

$$I\dot{\omega}(t) = -\gamma\omega(t) - k[\theta(t) - \theta_0(t)] + \sqrt{2\gamma T}\eta(t), \quad (1a)$$

$$\theta(t) = \int_0^t \omega(s) \quad (1b)$$

$$\theta_0(t) = \sqrt{2D_0} \int_0^t \eta_0(s) \quad (1c)$$

$$(1d)$$

where $\eta(t)$ and $\eta_0(t)$ are independent white normal Gaussian noises (unitary variance). The model represents the diffusion of a particle in a harmonic potential with “stiffness” k and unfixed minimum located at $\theta_0(t)$, under the effect of a thermal bath at temperature T and relaxation time I/γ . The harmonic potential, representing the cage created by the confining effect of the dense granular host fluid, is not fixed but moves, as $\theta_0(t)$ behaves as Brownian motion with diffusivity D_0 . Motivation for this model is twofold: 1) it reproduces the main features of the vpds, i.e. short time fast relaxation (region IV), an elastic resonance at intermediate times (region III) and a plateau revealing loss of memory at larger times (region II); 2) in the dilute limit (when $k \rightarrow 0$) it can be rigorously derived [29], 3) at intermediate densities a series of studies showed that memory effects (coming from correlated collisions) are well described by a similar coupling with an additional degree of freedom characterized by slower relaxation time-scales [23]. The vpds of the above model can be calculated and reads

$$S(f) = \frac{1}{\pi} \frac{D_0 k^2 + \gamma T (2\pi f)^2}{\gamma^2 (2\pi f)^2 + [k - I(2\pi f)^2]^2}. \quad (2)$$

Two limiting cases are recovered: when $k = 0$, the Ornstein-Uhlenbeck process is obtained, with $S(f)$ taking the Lorentzian form mentioned before. When $k > 0$ and $D_0 = 0$, one has the Klein-Kramers process in a fixed harmonic potential, and $S(f) \rightarrow 0$ for $f \rightarrow 0$, expressing the absence of diffusion at large times: the cage does not move and fully confines the particle. Formula (2) fairly fits the experimental spectra (see dashed lines in Fig. 1B) in regions II-IV, with $k/I \sim (2\pi \cdot 10)^2 \sim 4 \cdot 10^3 \text{ Hz}^2$ see [11]. Reasonably, the “cage stiffness” decreases at increasing shaking intensity. It also decreases as the density is reduced, and abruptly goes to zero at packing fractions of the order of $\sim 15\%$. The “cage diffusivity” D_0 rapidly increases with increasing Γ and with decreasing packing fraction (or number of particles).

The main problem of model (1) is that in region I it always predicts a diffusive behavior, no super-diffusion is allowed. In [11] superdiffusion was put in strict relation with a broad distribution of “inversion”, also called “persistence”, times measured with the following recipe. The frequencies of regions III and IV were filtered out, by considering a smoothed angular velocity $\omega_s(t) = \frac{1}{\tau} \int_0^\tau \omega(s) ds$

($\tau > 1s$), which displayed much smaller fluctuations than those of $\omega(t)$, but with positive correlation for very long times (larger than 10 s). This behavior, incompatible with model (1) (whose relaxation times are much smaller), is likely to be due to a quasi-steady motion of a large part of the granular medium surrounding and therefore dragging the probe. The large inertia is responsible for the observed long relaxation times. At high frequencies (part of region II, region III and IV) the contribution of $\omega_s(t)$ is negligible, explaining the good agreement with model (1) in that part of the spectrum.

In the following Section we propose an extension of this model, taking account the inertia of the surrounding medium, in order to reproduce the superdiffusive behavior.

III. THE ITINERANT OSCILLATOR MODEL WITH CAGE INERTIA

Motivated by the experimental measurement of long relaxation times, we introduce a new model to replace (or extend) that of Eq. (1):

$$I\dot{\omega}(t) = -\gamma\omega(t) - k[\theta(t) - \theta_0(t)] + \sqrt{2\gamma T}\eta(t) \quad (3a)$$

$$I_0\dot{\omega}_0(t) = -\gamma_0\omega_0(t) + k[\theta(t) - \theta_0(t)] + \sqrt{2\gamma_0 T_0}\eta_0(t) \quad (3b)$$

$$\theta(t) = \int_0^t \omega(t') dt' \quad (3c)$$

$$\theta_0(t) = \int_0^t \omega_0(t') dt'. \quad (3d)$$

In the above equations $\eta(t)$ and $\eta_0(t)$ are independent white gaussian noises with zero average and unitary variance, namely $\langle \eta(t)\eta(t') \rangle = \delta(t-t')$ and $\langle \eta_0(t)\eta_0(t') \rangle = \delta(t-t')$.

In equations (3) the angular velocity of the probe feels two different forces: of course they are both related to collisions, but one part is without memory and is described by the Ornstein-Uhlenbeck contribution $-\gamma\omega + \eta(t)$, while the second part takes the form $-k[\theta(t) - \theta_0(t)]$ and therefore depends upon the past history of $\omega(t)$ and $\omega_0(t)$. The choice of a harmonic interaction aims at simplifying the computations and can be justified by the small velocities of the blade with respect to that of the surrounding particles. The delaying force is modelled as a drag toward a reference point which slowly evolves in time, according to Eqs. (3b)-(3d). The variable $\theta_0(t)$ should be viewed as a collective degree of freedom representing the preferential point of the blade with respect to some granular *cage*. The *cage* slowly changes its configuration and favours the blade’s drift at later times.

In the previous, simpler, model, Eq. (1), the dynamics of $\theta_0(t)$ was *overdamped*, as in a motion without inertia. The new model takes into account the crucial effect of cage inertia, through the introduction of a fourth degree of freedom $\omega_0(t) = \dot{\theta}_0$ which evolves with Eq. (3b), as

well as the effect of the blade upon the granular material through the reciprocal elastic drag. This last ingredient is likely to be negligible, in view of the large value of the inertia I_0 , but its inclusion is convenient for symmetry and physical consistency. We must emphasize that this model can be understood in the context of other models, often referred to as “two temperature models” (see [30, 31] and references therein), where a particle moves under the influence of different thermostats acting at different timescales. Even if it is quite natural, in dissipative systems such as a granular fluid, to associate different temperatures to different timescales, in the following we show that the main subject of our study, which is superdiffusion, can be obtained even for equal temperatures.

Introduction of cage inertia is the main novelty with respect to the original Itinerant Oscillator model, including the version discussed in [11], and certainly deserves some motivation. At low temperatures, activated processes (that is the possibility to “jump out” of the cage thanks to some thermal fluctuation) are negligible and the probe never really escapes from a cage: on the contrary, it is the cage that slowly evolves and dictates the motion of the probe at large times. A displacement of the probe $\Delta\theta(t)$ between two instants separated by a large time t , therefore, is closely related to a displacement $\Delta\theta_0(t)$ of the cage itself, i.e. of a large part of the surrounding granular medium. Then it is reasonable, when looking for an ingredient reproducing almost ballistic superdiffusion, to imagine that the cage is doing long ballistic drifts (at very small velocity), sustained by its large inertia. Discreteness and finiteness of the granular material, which in the experiments is made of a few thousands grains, makes random but persistent (also called “secular” [32]) drifts possible. For those reasons it seems reasonable to us the introduction of a large “cage inertia” I_0 . The event of a large portion of solvent to drift in a particular direction for times larger than the cage relaxation is highly unlikely in a dense molecular liquid: this explains why one usually do not observe superdiffusion in ordinary liquids. It is out of the scope of the present paper to discuss the exact mechanism of formation of the large cage inertia I_0 in a vibrated granular medium, as well as the reason why it increases when the vibration amplitude is reduced [33]. The answers to such questions are postponed to future investigations: our main aim, here, is to convince the reader that the concept of “cage inertia” is useful for the description of low temperature granular liquids.

The model is linear and it is useful to recast it into a more compact form, by defining the vector $w(t) = \{z(t), \omega(t), \omega_0(t)\}$, with $z(t) = \theta(t) - \theta_0(t)$. The model then takes the form

$$\dot{w} = -Aw + B\tilde{\eta}(t), \quad (4)$$

	I	T	γ	k	I_0	T_0	γ_0
case A	1	1	100	0	/	/	/
case B	1	1	100	5000	0	0.1	1000
case C	1	1	100	5000	10	0.1	1000
case D	1	1	100	5000	10^3	100	10
case E	1	1	100	5000	10^4	100	10
case F	1	1	100	5000	10^4	1	10

TABLE I. Values of the parameters for the cases illustrated in the paper. A: The Ornstein-Uhlenbeck process. B: A case without cage inertia (overdamped cage). C, D, E: cases with small, medium or large cage inertia. F: equal to case E, but at thermodynamic equilibrium $T_0 = T$.

with

$$A = \begin{pmatrix} 0 & -1 & 1 \\ \frac{k}{T} & \frac{\gamma}{T} & 0 \\ -\frac{k}{I_0} & 0 & \frac{\gamma_0}{I_0} \end{pmatrix}, \quad (5)$$

$$B = \begin{pmatrix} 0 & 0 & 0 \\ 0 & \frac{\sqrt{2\gamma T}}{T} & 0 \\ 0 & 0 & \frac{\sqrt{2\gamma_0 T_0}}{I_0} \end{pmatrix}, \quad (6)$$

$$\tilde{\eta} = \begin{pmatrix} 0 \\ \eta(t) \\ \eta_0(t) \end{pmatrix}. \quad (7)$$

The analysis of the model will be discussed focusing on a few particular cases, inspired by the experimental results of [11], which are listed in Table I. By fixing $I = 1$ and $T = 1$, the units of moment of inertia and time are fixed. A comparison with experimental observations suggests that our arbitrary time unit is close to 1 real second. In Table I, case A is similar to a dilute experiment, while cases D or E are similar to a dense and cold one. Case B is an example of cage without inertia ($I_0 = 0$), which cannot display superdiffusion. Case C is similar to that, as I_0 is small. Finally Case F has still a large cage inertia, but has the peculiarity to be at thermodynamic equilibrium, i.e. $T_0 = T$. Nevertheless, we will see that this ingredient is relevant only in the study of Fluctuation-Dissipation relation and has no consequences for the presence of cages or superdiffusion, as it does not crucially affect the timescales of relaxation.

IV. STATICS: ONE TIME QUANTITIES IN THE STATIONARY STATE

Eqs. (4) constitute a linear system, which is solved by Gaussian multivariate distributions. We assume that the values of the parameter of the model are such that only eigenvalues with positive real part appear and a steady state can be reached. In such a steady state, the one time distribution function takes the form

$$P(z, \omega, \omega_0) = \frac{1}{\sqrt{(2\pi)^3 \det(\sigma)}} \text{Exp} \left[-\frac{1}{2} w^T \beta w \right] \quad (8)$$

where $\beta = \sigma^{-1}$ and σ is the covariance matrix, which we write in the form

$$\sigma = \begin{pmatrix} \sigma_{zz} & \sigma_{z\omega} & \sigma_{z\omega_0} \\ \sigma_{z\omega} & \sigma_{\omega\omega} & \sigma_{\omega\omega_0} \\ \sigma_{z\omega_0} & \sigma_{\omega\omega_0} & \sigma_{\omega_0\omega_0} \end{pmatrix}. \quad (9)$$

The covariance matrix satisfies the equation [34]

$$A\sigma + \sigma A^T = BB, \quad (10)$$

which is rewritten as

$$\sigma_{z\omega} = \sigma_{z\omega_0} \quad (11a)$$

$$I(\sigma_{\omega\omega_0} - \sigma_{\omega\omega}) + k\sigma_{zz} + \gamma\sigma_{z\omega} = 0 \quad (11b)$$

$$I_0(\sigma_{\omega_0\omega_0} - \sigma_{\omega\omega_0}) - k\sigma_{zz} + \gamma_0\sigma_{z\omega_0} = 0 \quad (11c)$$

$$I(k\sigma_{z\omega} + \gamma\sigma_{\omega\omega}) = T\gamma \quad (11d)$$

$$I_0(\gamma_0\sigma_{\omega_0\omega_0} - k\sigma_{z\omega_0}) = T_0\gamma_0 \quad (11e)$$

$$\frac{k\sigma_{z\omega_0} + \gamma\sigma_{\omega\omega_0}}{I} + \frac{\gamma_0\sigma_{\omega\omega_0} - k\sigma_{z\omega}}{I_0} = 0. \quad (11f)$$

The solution reads

$$\sigma_{\omega\omega} = \frac{T}{I} - \gamma_0(T - T_0) \frac{A_1}{d} \quad (12a)$$

$$\sigma_{\omega_0\omega_0} = \frac{T_0}{I_0} + \gamma(T - T_0) \frac{A_1}{d} \quad (12b)$$

$$\sigma_{zz} = \frac{T}{k} - (T - T_0) \frac{A_2}{d} \quad (12c)$$

$$\sigma_{\omega\omega_0} = (T - T_0) \frac{A_3}{d} \quad (12d)$$

$$\sigma_{z\omega} = \sigma_{z\omega_0} = (T - T_0) \frac{A_4}{d}, \quad (12e)$$

with $A_1 = k(\gamma_0 I + \gamma I_0)$, $A_2 = \frac{\gamma_0(I^2 k(\gamma + \gamma_0) + \gamma^2 \gamma_0 I + \gamma^3 I_0)}{k}$, $A_3 = \gamma \gamma_0 k(I - I_0)$, $A_4 = \gamma \gamma_0(\gamma_0 I + \gamma I_0)$ and $d = (\gamma + \gamma_0)(\gamma_0 I^2 k + \gamma \gamma_0^2 I + \gamma I_0^2 k + \gamma^2 \gamma_0 I_0)$.

We can recover two well known physical limits. In the decoupling limit $k \rightarrow 0$, one has

$$\sigma_{\omega\omega} = \frac{T}{I} \quad (13a)$$

$$\sigma_{\omega_0\omega_0} = \frac{T_0}{I_0} \quad (13b)$$

$$\sigma_{zz} = \infty \quad (13c)$$

$$\sigma_{\omega\omega_0} = 0 \quad (13d)$$

$$\sigma_{z\omega} = \sigma_{z\omega_0} = \frac{T - T_0}{\gamma + \gamma_0}. \quad (13e)$$

It is important to note that this limit is singular (since the case $k = 0$, corresponding to two independent Ornstein-Uhlenbeck processes, is non-stationary for z): this explains why $\sigma_{z\omega} = \sigma_{z\omega_0} \neq 0$.

For $T = T_0$, that is at thermodynamic equilibrium, one

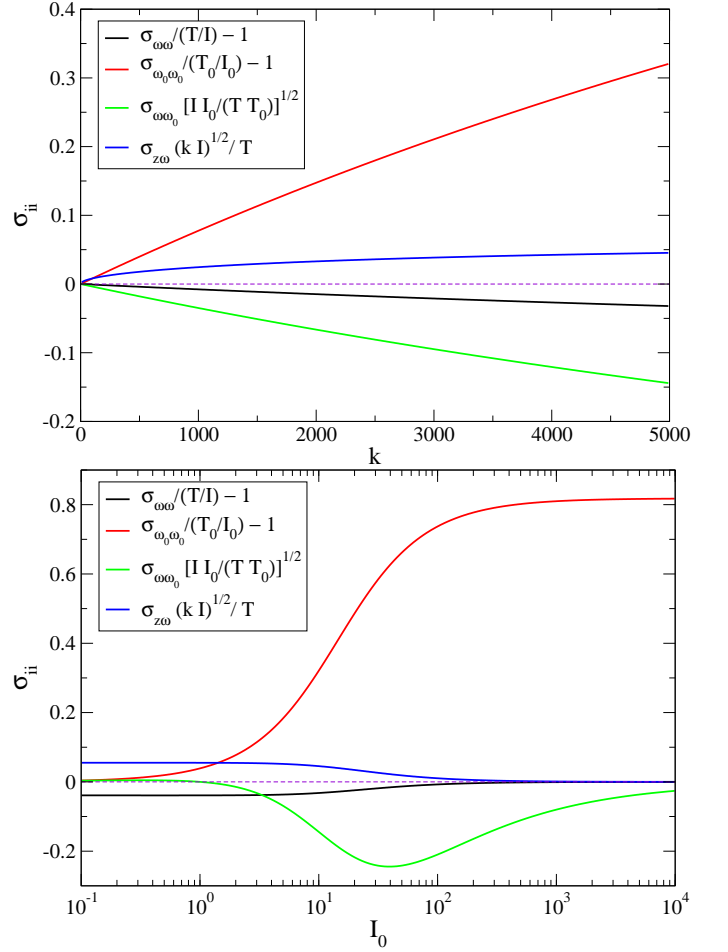


FIG. 2. We show how σ_{ii} (for some i , i.e. ω , ω_0 and z , properly normalized) depend on k or I_0 , while all the other parameters are fixed according to case C of Table I. On the top panel, we see the important effect of the coupling quantity k on both self-correlations and cross-correlations. On the bottom one, we notice that the effect of cage inertia I_0 on the coupling (e.g. $\sigma_{\omega\omega_0}$, green curve), is larger for intermediate values: at smaller values $\sigma_{\omega_0\omega_0}$ is close to its “uncoupled” value, while it deviates from it at large values; the opposite happens to $\sigma_{\omega\omega}$.

has

$$\sigma_{\omega\omega} = \frac{T}{I} \quad (14a)$$

$$\sigma_{\omega_0\omega_0} = \frac{T}{I_0} \quad (14b)$$

$$\sigma_{zz} = \frac{T}{k} \quad (14c)$$

$$\sigma_{\omega\omega_0} = 0. \quad (14d)$$

$$\sigma_{z\omega} = \sigma_{z\omega_0} = 0. \quad (14e)$$

In Fig. 2, we have reproduced the values of the most relevant covariances as a function of k or I_0 in a case with $T \neq T_0$. The coupling k produces a shift of the two “temperatures” $I\sigma_{\omega\omega}$ and $I_0\sigma_{\omega_0\omega_0}$. It also produces

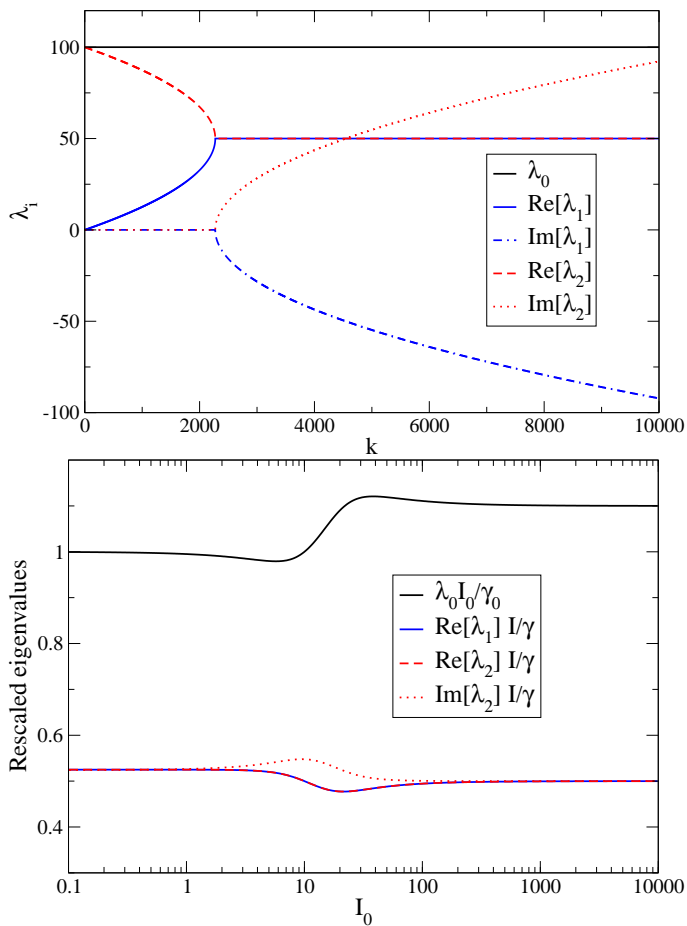


FIG. 3. The three eigenvalues of matrix A as a function of k or I_0 . The other parameters are fixed as in case C of Table I. It is interesting to see that the experimental observations in [11] occurred in the region beyond the bifurcation, i.e. the one with complex eigenvalues.

the appearance of cross correlations $\sigma_{\omega\omega_0}$: it is crucial to note, from Eq. 14, that such cross correlation is empty in the equilibrium case, even in the presence of the coupling $k > 0$.

V. DYNAMICS

A. Characteristic times

The dynamics is characterized by three relaxation times, which are the inverse of the eigenvalues of matrix A . The latter are the zeroes of the characteristic (cubic) polynomial: a compact expression is not available in general. The equation for the eigenvalues reads

$$-\lambda^3 + B_2\lambda^2 - B_1\lambda + B_0 = 0, \quad (15)$$

with

$$B_2 = \frac{\gamma_0 I + \gamma I_0}{II_0} \quad (16a)$$

$$B_1 = \frac{\gamma_0 \gamma + k(I + I_0)}{II_0} \quad (16b)$$

$$B_0 = k \frac{\gamma_0 + \gamma}{II_0}. \quad (16c)$$

For the solutions to be complex or not, the value of the discriminant must be compared to zero:

$$\Delta = 18B_2B_1B_0 - 4B_2^3B_0 + B_2^2B_1^2 - 4B_1^3 - 27B_0^2. \quad (17)$$

If $\Delta < 0$ there are one real and two complex conjugated eigenvalues. If $\Delta \geq 0$ the eigenvalues are all real. Therefore a bifurcation point appears when $\Delta = 0$ and this happens depending on the values of $\gamma_0, \gamma, k, I, I_0$. We do not intend to exhaust all the possibilities. In Figure 3 we have reported a plot of the eigenvalues when k or I_0 are varied, keeping constant all the other parameters. The bifurcation when k is increased is quite evident. It is interesting to notice that a comparison with experimental data, see [11] where $k/I \sim 4 \cdot 10^3$, suggests values of the parameter in the phase with complex eigenvalues.

It should be noted that, even when all eigenvalues are real, the correlation functions (discussed in details below) can show non-monotonic behavior because of the superposition of exponentials with different characteristic times and with positive/negative coefficients. The appearance of complex eigenvalues is a source of persistent oscillatory behavior in the correlation function, which is of course always damped at large time by the exponential with remaining real eigenvalue.

B. Velocity power density spectrum

In this section we study the vpds for the probe's angular velocity $\omega(t)$, which is defined as

$$S(f) = \lim_{t_{TOT} \rightarrow \infty} \frac{1}{2\pi t_{TOT}} \left| \int_0^{t_{TOT}} \omega(t) e^{2\pi f i t} dt \right|^2, \quad (18)$$

which is also equivalent to the Fourier transform of the autocorrelation function in the steady state $\langle \omega(t)\omega(0) \rangle$ (see next Section for a discussion). In the following, to avoid confusion with the probe's angular velocity $\omega(t)$, we will use the symbol $f = 2\pi f$ to denote the angular frequency associated with f , whose use makes more compact the formula.

By time-Fourier-transforming Eqs. (3) and taking the squared modulus, the following formula for the vpds is obtained:

$$S(\bar{f}) = \frac{1}{\pi} \frac{\gamma T [k^2 + \bar{f}^2(\gamma_0^2 - 2kI_0) + \bar{f}^4 I_0^2] + \gamma_0 T_0 k^2}{k^2(\gamma + \gamma_0)^2 + \bar{f}^2 \{k[(I + I_0)^2 k - 2I_0 \gamma^2] + (\gamma^2 - 2Ik)\gamma_0^2\} + \bar{f}^4 [I_0^2 \gamma^2 - 2II_0^2 k + I^2(\gamma_0^2 - 2I_0 k)] + \bar{f}^6 I^2 I_0^2}. \quad (19)$$

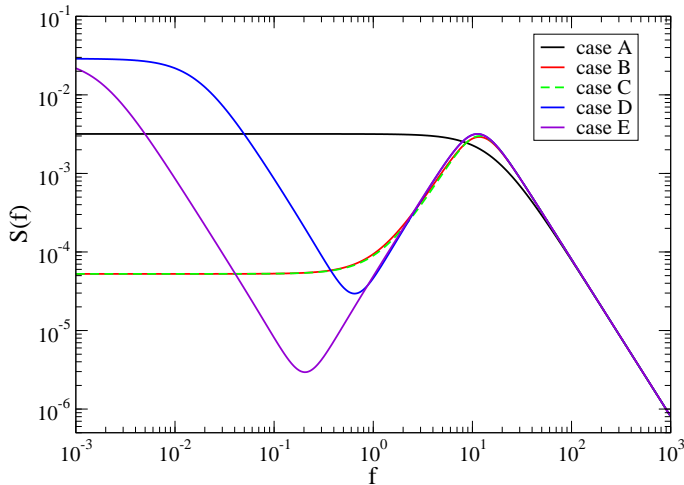


FIG. 4. Velocity power density spectrum (vpds) for some cases. The parameters of the model are illustrated in Table I. The usual Lorentzian vpds is observed for the uncoupled case A, while for the coupling case with zero or small cage inertia (cases B and C) we recover the same shape (plateau followed by a bump) as in the “overdamped model” discussed in [11]. In cases D and E, that is with non negligible cage inertia I_0 , a region on the left of the resonant bump appears with a power law decay resembling experimental observations at small f [11].

The formula is quite rich and may correspond to very different shapes depending on the choices of the many parameters. We are motivated by a qualitative comparison with the experimental shapes, see Fig. 1B, and for this reason restrict our study to a few paradigmatic choices of parameters listed in Table I.

In Fig. 4 the numerical computation of formula (19) is displayed for such choices. As expected, case A (no coupling, typical of dilute gases) reproduces the classical Lorentzian form for the spectrum of the Ornstein-Uhlenbeck process, as verified by substituting $k = 0$ in Eq. (19) which gives

$$S(\bar{f}) = \frac{T\gamma}{\pi(\bar{f}^2 I^2 + \gamma^2)}. \quad (20)$$

Case B is similar to the model used in [11]: it shows the resonant bump due to the cage effect, but is forced to a plateau in the region at low \bar{f} , because of the vanishing cage’s inertia, i.e. $I_0 = 0$ (no superdiffusion). This choice corresponds to an “overdamped” dynamics for the collective degree of freedom θ_0 , and analytically gives

$$S(\bar{f}) = \frac{1}{\pi} \frac{k^2(T\gamma + T_0\gamma_0) + \bar{f}^2 T \gamma \gamma_0^2}{k^2(\gamma + \gamma_0)^2 + \bar{f}^2 [I^2 k^2 + \gamma_0^2(\gamma^2 - 2Ik)] + \bar{f}^4 I^2 \gamma_0^2}. \quad (21)$$

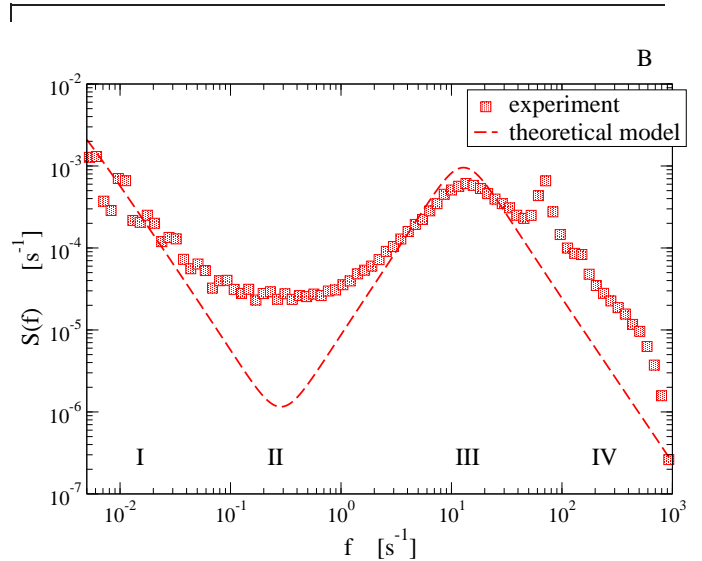


FIG. 5. Here, we show a comparison between the theory, Eq. (19) (dashed lines) and the experimental data (symbols) of the velocity power density spectrum (vpds). The parameters of the theory are $T = 0.3$, $I = 1$, $\gamma = 100$, $k = 6500$, $T_0 = 70$, $I_0 = 10^4$, $\gamma_0 = 10$, which are close to case E. The experimental data come from Ref. [11], in the cold liquid case.

The expression is the analogue of the one reported in [11], with the (not crucial) novelty that here $\theta_0(t)$ is also subject to the reciprocal of the coupling elastic force.

Case C is similar to B, since I_0 , even if finite, is still small. Case D and E, on the contrary, exhibit the effect of growing cage inertia and therefore an increasing behavior as $\bar{f} \rightarrow 0$. In both cases, necessarily, $S(\bar{f})$ becomes flat at very small \bar{f} , since all characteristic times - even if large - are finite. From Fig. 4 it is clear that the effect of I_0 is crucial: it rules the larger relaxation time and determines the duration of “anomalous” part of the spectrum.

It is interesting to realize that the ramp at small values of \bar{f} in cases D and E has a $\sim \bar{f}^{-2}$ behavior which resembles the high \bar{f} region. This is reasonable as ω , at small frequencies, is somehow enslaved by the dynamics of ω_0 : the latter is, basically, a Ornstein-Uhlenbeck process realized at much longer timescales. This is also the elementary reason why the mean squared displacement, as discussed below and as observed in some experiments [11], is close to ballistic.

In Fig. 5 we can observe that our model - even if reproducing, in cases with large cage inertia (D and E), the ramp at small f associated with super-diffusion - does not do a perfect job in reproducing the whole shape of the experimental vpds. Indeed, the experimental observations suggest that the crossover from the cage bump to the ramp at small f is much smoother, basically flat: our model, on the contrary, predicts (independently from

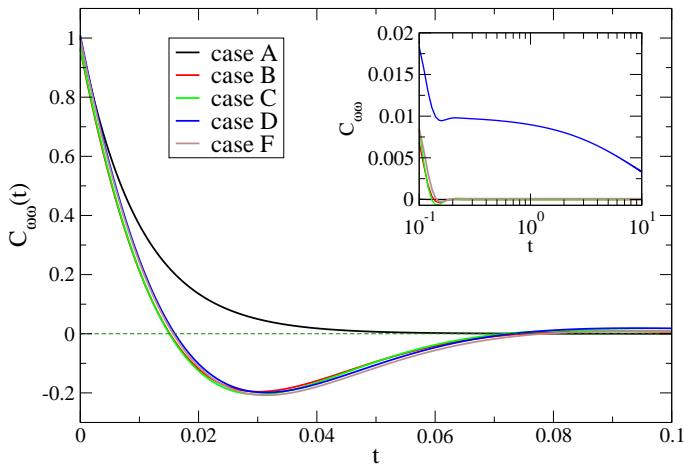


FIG. 6. Autocorrelations $C_{\omega\omega}(t)$ for some choices of parameters, as illustrated in Table I. The inset shows the same autocorrelations at larger time, in order to highlight the persistent behavior of cases with high cage inertia I_0 (D and F). Interestingly, the cage inertia I_0 does not affect in a relevant way the behavior of the autocorrelation at time smaller than 0.1. Case E, very close to the F one (different temperatures do not affect the qualitative shape of the autocorrelation), is not shown for the sake of clarity

the parameters) a deep elbow. It is not possible to find any region in the parameter space where a plateau appears as in the experiment, namely, there is always a sharp minimum for the $S(f)$ near the local maximum. Our conjecture is that, in order to reproduce the smooth crossover, the noise $\eta_0(t)$ should be modified, possibly replaced by some coloured stochastic process. Notwithstanding this discrepancy, we will see in the next section that our theory fits very well the behavior of the mean square displacement.

C. Autocorrelations and mean squared displacement

The two-time covariance matrix in steady state, which is time-translational invariance, reads

$$C_{ij}(t) \stackrel{\text{def}}{=} \langle w_i(t)w_j(0) \rangle = \exp(-At)C_{ij}(0). \quad (22)$$

A compact expression of $\exp(-At)$ is out of question, as already discussed for the eigenvalues. We recall that $C_{\omega\omega}(t) \stackrel{\text{def}}{=}} C_{22}(t) = \langle \omega(t)\omega(0) \rangle$ can also be obtained by the inverse Fourier transform of the vpds. This is true for each component of $C_{ij}(t)$ which is related - through transforms - to the cross-spectrum.

Autocorrelations for some choices of the parameters are numerically computed (from analytical formula) and shown in Fig. 6. It is evident the passage from a simple exponential decay of uncoupled case A ($k = 0$) to the “back-scattering” behavior, typical of cages in liquid, in

all other cases with $k \neq 0$. The cage’s inertia I_0 does not change in a crucial way the behavior of the first part of the autocorrelation, but determines a larger and larger persistency of correlations at late times, as seen in the inset. It is important to realize that the value of the autocorrelation at large time, even if not vanishing, is very small with respect to its order of magnitude at small times.

From the knowledge of $C_{\omega\omega}(t)$, it is possible to compute the time-evolution of the mean squared displacement (msd):

$$\begin{aligned} \langle [\Delta\theta(t)]^2 \rangle &= \int_0^t dt' \int_0^t dt'' \langle \omega(t')\omega(t'') \rangle \\ &= 2 \int_0^t dt' (t-t')C_{\omega\omega}(t'). \end{aligned} \quad (23)$$

In Figure 7 we show, for a few choices of the parameters, the behavior of the msd. The uncoupled case A reproduces the standard ballistic-diffusive dynamics which is typical of diffusion in dilute gases. Coupling ($k > 0$) induces a dynamical arrest in the form of a plateau in the msd, which - later - is overcome by the slow cage dynamics. Such dynamics is purely diffusive in the case without inertia ($I_0 = 0$ or small) while it is super-diffusive when I_0 is large. When the observation time is larger than the time dictated by I_0 (basically I_0/γ_0) the msd comes back to normal diffusion. In experiments such a very late stage was observed on timescale of the order of hours, see Supplemental Material in [11]. We wish to underline that, how anticipated, the equilibrium case F - which differs from case E just in the fact that the temperatures are equal ($T = T_0$) - displays superdiffusion as well. The long memory is induced by the large cage inertia I_0 and is not related to the system being at equilibrium or out of it.

To conclude this Section, in Fig. 8 we show an excellent agreement for the msd between theory and experiment in a cold liquid case. The superposition is fair along all the timescales.

D. Persistency.

An intriguing counterpart of super-diffusion is a long memory in the velocity variable $\omega(t)$. At times shorter than the typical time needed to overcome the cage effect, the dynamics of $\omega(t)$ is dominated by rapid intracage oscillations and fast thermal relaxation. As seen in Fig. 6, when cage inertia is large the autocorrelation of $\omega(t)$ displays a very small long-lasting drift. Such a weak signal in the autocorrelation disappears, in experiments, because of noise. A better observable [11], is the distribution of inversion times for the slow part of the signal, which is strictly connected to such a long memory. In order to make contact with the experimental results in [11], we have studied this distribution in our theoretical model. To remove the effect of rapid relaxation,

we apply a filter and study $\omega_s(t) = \frac{1}{\tau} \int_t^{t+\tau} ds \omega(s)$, using values of $\tau = 2$ larger than the cage relaxation time. An inversion time t_{inv} is the time between two zeroes of $\omega_s(t)$. The inversion times, therefore, represent the duration of “persistence” of the direction of motion. We remark that a theoretical computation of the distribution of persistency times is a tough task which we have not pursued here. On the contrary, we have simulated numerically the model (3) and we have computed the

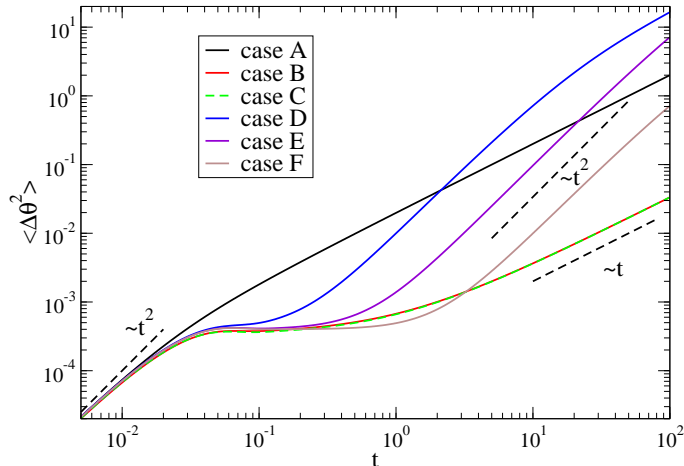


FIG. 7. Mean square displacement for some choices of the parameters, as illustrated in Table I. The phenomena observed in the vpd’s are also observed in the MSD. After a common ballistic regimes, all cases with coupling (i.e. excluding case A) show an intermediate cage effect visible as brief plateau. After the plateau the cases with zero or small cage inertia I_0 (B and C) show normal diffusion, while the cases with large cage inertia (D and E) present ballistic super-diffusion. The super-diffusive behavior terminates at a time which is larger as I_0 increases.

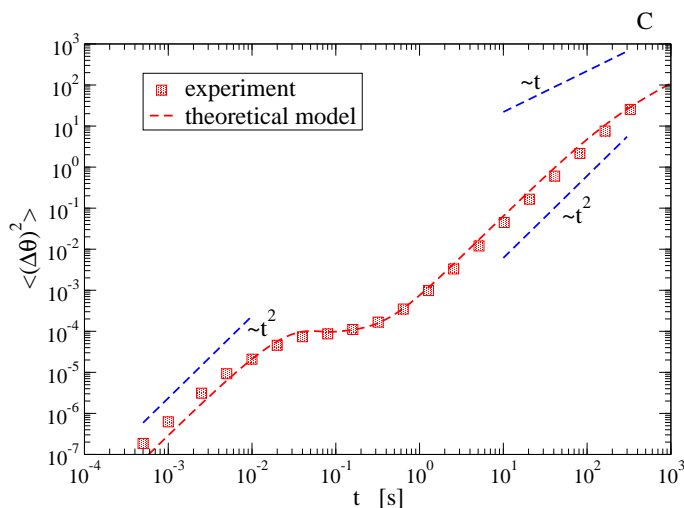


FIG. 8. Comparison between the theory (dashed lines) and the experimental data (symbols) for the mean square displacement for the same case of Fig. 5.

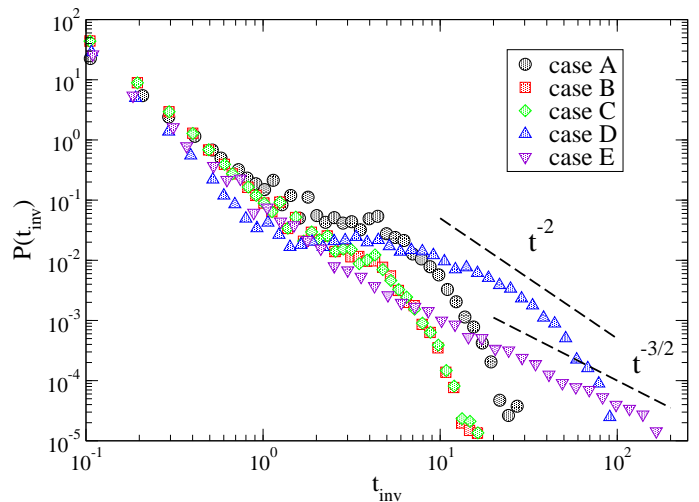


FIG. 9. Distributions of inversion times for some of the cases in Table I. All distributions present a - more or less visible - cut-off at a finite time. Looking at the coupled case (B-E), it is seen that when the cage inertia I_0 is increased, the cut-off time increases too. In the cases with largest cage inertia (D and E), the cut-off time is large enough to “uncover” some power-law decay. In order to present more clearly the results, and given that cases E and F are very close, we show only case E.

distribution $P(t_{inv})$, which is shown in Fig. 9. From this plot one immediately appreciates the role of cage inertia I_0 in inducing large inversion times. Uncoupled case (A) as well as the coupled cases with zero or low inertia (B and C) show a distribution of t_{inv} with a fast decay at a small cut-off time. When the cage inertia I_0 is increased, the distribution develops a large tail $\sim t_{inv}^{-\alpha}$ whose cut-off increases, while $\alpha \leq 2$. It is interesting to notice that similar exponents have been observed in the experimental distribution, where they were in perfect agreement with superdiffusion predicted by a continuous time random walk model for $\omega_s(t)$ [11].

E. Linear response

The aim of this section is to study the response of the variable $\omega(t)$ to the application of a force (torque) upon it. As the model is linear, the response is always linear. However we do not believe that the model can reproduce experimental observations when a large force is applied, i.e. in the non-linear regime it should be properly modified.

The dynamical response matrix simply reads $R(t) = \exp(-At)$. Therefore $R_{\omega\omega}(t) \stackrel{def}{=} R_{22}(t) = \frac{\delta\omega(t)}{\delta\omega(0)}$. It is interesting to notice that the same expression is obtained by applying the Generalized Fluctuation-Response Relation discussed in [35, 36]:

$$\frac{\delta\omega(t)}{\delta\omega(0)} = - \left\langle \omega(t) \frac{\partial \ln P(z, \omega, \omega_0)}{\partial \omega} \Big|_{t=0} \right\rangle \quad (24)$$

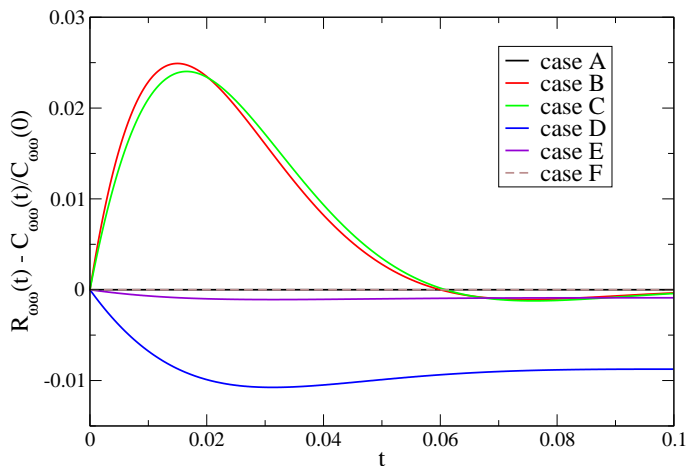


FIG. 10. Deviation from equilibrium measured as a distance from the Einstein relation, in some cases from the list in Table I. There is no deviation in the uncoupled case (A) and in the coupled case when $T = T_0$ (F). All other cases show a deviation from the Einstein relation of similar order of magnitude, with the exception of the large cage inertia case (E) which is quite smaller.

where $P(z, \omega, \omega_0)$ is the unperturbed steady state distribution, Eq. (8) in our case. Applying the results of Sec. IV, we get, therefore:

$$\frac{\delta\omega(t)}{\delta\omega(0)} = \beta_{\omega\omega}\langle\omega(t)\omega(0)\rangle + \beta_{\omega\omega_0}\langle\omega(t)\omega_0(0)\rangle + \beta_{z\omega}\langle\omega(t)z(0)\rangle, \quad (25)$$

where we remind that $\beta = \sigma^{-1}$ is the inverse covariance matrix. Such an expression makes clear the role of static correlations, which is the crucial ingredient modifying the equilibrium Fluctuation-Response relation [23, 37–39]

Indeed, from expression (25) and Eqs. (12), it appears that at equilibrium, i.e. when $T = T_0$ (with or without coupling) one has $R_{\omega\omega}(t) = C_{\omega\omega}(t)/C_{\omega\omega}(0)$, which is a way to express the so-called Einstein relation which gives mobility as proportional to diffusivity. Plots of the difference between the response $R_{\omega\omega}(t)$ and the rescaled autocorrelation $C_{\omega\omega}(t)/C_{\omega\omega}(0)$ are shown in Fig. 10. When $T \neq T_0$ (and $k > 0$) the response is always different from the rescaled autocorrelation and the Einstein relation is always violated. An experiment comparing linear response to autocorrelation would be able to put in evidence the distance from equilibrium in the system.

VI. CONCLUSIONS AND PERSPECTIVES

The theoretical understanding of the liquid state of granular fluids is in an underdeveloped stage, if com-

pared with granular gases or with slowly tapped/sheared (or even static) granular “solids”. The situation could be considered similar to the theory of liquids in the 60’s, where neutron scattering spectra were explained by proposing super-simplified models [25, 26].

In this spirit, here we have proposed a simple model which reproduces two striking features of a recent experiment [11], namely: a transient dynamical arrest (cage effect), and late time - almost ballistic - superdiffusion. A qualitative comparison with the experimental results is fair for the velocity power density spectrum, as it includes the “resonant” bump associated with the cage effect and the strong enhancement at low frequencies ($f \rightarrow 0$) which seems related to superdiffusion. The comparison for the mean squared displacement is even more striking, and shows how the superdiffusive behavior emerges only when the “cage inertia” I_0 is large. In close analogy with the experiments, also the distribution of persistency times is strongly affected by the value of I_0 which controls the cut-off time of the distribution and the possibility to observe slow (power-law) decays. We have also discussed how the lack of thermal equilibration between $\omega(t)$ and the collective variable $\omega_0(t)$, which is a common feature of granular fluids due to non-conservative interactions, could be demonstrated in future experiments through an analysis of linear response.

As a concluding remark, we wish to underline that the model proposed is purely phenomenological and lacks a general derivation from first principles. In particular, the experimental parameters such as the packing fraction or the average energy input do not enter in this simplified picture and there is no way to deduce or estimate a reasonable value for I_0 . The experimental observations suggest that, when the “granular temperature” is decreased, larger and larger values of I_0 are realised. Tentative fits of experimental vpds at the smallest granular temperatures, with the formula derived here, give the values of the “collective” momentum of inertia of $I_0 \sim 10^4 I$: if we assume that this is the momentum of inertia of a solid made of a material density of steel (as the granular spheres) reduced by the packing fraction (order $\sim 50\%$) it gives a radius of the order of 10^2 mm which matches the order of magnitude of the size of the container filled by grains in the experiment. A mechanism explaining the building up of cage inertia is still lacking and certainly deserves future investigation.

ACKNOWLEDGMENTS

The authors acknowledge useful discussions with A. Gnoli, A. Sarracino and A. Vulpiani, and especially thank A. Gnoli and C. Scalliet for the experimental data.

[1] H. M. Jaeger, S. R. Nagel, and R. P. Behringer, *Physics Today* **49**, 32 (1996).

[2] A. Baldassarri, A. Puglisi, and A. Sarracino, C. R.

- Physique **16**, 291 (2015).
- [3] B. Andreotti, Y. Forterre, and O. Pouliquen, *Granular Media. Between Fluid and Solid* (Cambridge University Press, 2013).
- [4] S. Luding, Nonlinearity **22**, R101 (2009).
- [5] A. Fiege, T. Aspelmeier, and A. Zippelius, Phys. Rev. Lett. **102**, 098001 (2009).
- [6] N. K. Brilliantov and T. Poschel, *Kinetic Theory of Granular Gases* (Oxford University Press, 2004).
- [7] A. Puglisi, *Transport and Fluctuations in Granular Flows* (Springer-Verlag, 2015).
- [8] A. Prados, A. Lasanta, and P. I. Hurtado, Physical Review E **86**, 031134 (2012).
- [9] G. D’Anna, P. Mayor, A. Barrat, V. Loreto, and F. Nori, Nature **424**, 909 (2003).
- [10] G. H. Wortel, J. A. Dijksman, and M. van Hecke, Phys. Rev. E **89**, 012202 (2014).
- [11] C. Scalliet, A. Gnoli, A. Puglisi, and A. Vulpiani, Phys. Rev. Lett. **114**, 198001 (2015).
- [12] J. C. Dyre, Rev. Mod. Phys. **78**, 953 (2006).
- [13] C. Heussinger, L. Berthier, and J.-L. Barrat, Europhys. Lett. **90**, 20005 (2010).
- [14] F. Lechenault, O. Dauchot, G. Biroli, and J. P. Bouchaud, Europhys. Lett. **83**, 46003 (2008).
- [15] A. Cavagna, Phys. Rep. **476**, 51 (2009).
- [16] G. Marty and O. Dauchot, Phys. Rev. Lett. **94**, 015701 (2005).
- [17] P. M. Reis, R. A. Ingale, and M. D. Shattuck, Phys. Rev. Lett. **98**, 188301 (2007).
- [18] B. Utter and R. P. Behringer, Phys. Rev. E **69**, 031308 (2004).
- [19] F. Radjai and S. Roux, Phys. Rev. Lett. **89**, 064302 (2002).
- [20] R. Klages, G. Radons, and I. M. Sokolov, eds., *Anomalous transport* (Wiley&Sons, 2008).
- [21] J. Klafter, S. C. Lim, and R. Metzler, eds., *Fractional Dynamics: Recent Advances* (World Scientific, 2012).
- [22] K. Andersen, P. Castiglione, A. Mazzino, and A. Vulpiani, Eur. Phys. J. B **18**, 447 (2000).
- [23] A. Sarracino, D. Villamaina, G. Gradenigo, and A. Puglisi, Europhys. Lett. **92** (2010).
- [24] A. Rahman, Physical Review **136**, A405 (1964).
- [25] V. F. Sears, Proc. Phys. Soc. **86**, 953 (1965).
- [26] W. Coffey, Y. P. Kalmykov, and J. T. Waldron, *The Langevin Equation: With Applications in Physics, Chemistry, and Electrical Engineering* (World Scientific, 1996).
- [27] H. D. Vollmer, Z. Physik **33**, 103 (1979).
- [28] E. Fodor, K. Kanazawa, H. Hayakawa, P. Visco, and F. van Wijland, Phys. Rev. E **90**, 042724 (2014).
- [29] A. Sarracino, D. Villamaina, G. Costantini, and A. Puglisi, J. Stat. Mech. **2010**, P04013 (2010).
- [30] L. F. Cugliandolo and J. Kurchan, J. Phys. Soc. Jpn. **69**, 257.
- [31] D. O. Soares-Pinto and W. A. M. Morgado, Phys. Rev. E **77**, 011103 (2008).
- [32] A. Pons, A. Amon, T. Darnige, J. Crassous, and E. Clément, “Mechanical fluctuations suppress the threshold of soft-glassy solids : the secular drift scenario,” (2014), unpublished, preprint at arXiv:1412.3288.
- [33] M. Cencini, M. Falcioni, D. Vergni, and A. Vulpiani, Physica D **130**, 58 (1999).
- [34] C. W. Gardiner, *Handbook of stochastic methods* (Springer Berlin, 1985).
- [35] G. S. Agarwal, Z. Physik **252**, 25 (1972).
- [36] U. M. B. Marconi, A. Puglisi, L. Rondoni, and A. Vulpiani, Physics Reports **461**, 111 (2008).
- [37] D. Villamaina, A. Baldassarri, A. Puglisi, and A. Vulpiani, J. Stat. Mech. **2009**, P07024 (2009).
- [38] A. Crisanti, A. Puglisi, and D. Villamaina, Physical review. E, Statistical, nonlinear, and soft matter physics **85**, arXiv:arXiv:1202.0508v1.
- [39] A. Gnoli, A. Puglisi, A. Sarracino, and A. Vulpiani, Plos One **9**, e93720 (2014).